Florian Straube, Frank Schultz, Michael Makarski, Stefan Weinzierl

Optimized Driving Functions for Curved Line Source Arrays Using Modeled and Measured Loudspeaker Data

Straube, Florian; Schultz, Frank; Makarski, Michael; Weinzierl, Stefan (2016): Optimized Driving Functions for Curved Line Source Arrays Using Modeled and Measured Loudspeaker Data. In: Proceedings of the Inter-Noise 2016 : 45th International Congress and Exposition on Noise Control Engineering : towards a quiter future : August 21-24, 2016, Hamburg. Berlin: Deutsche Gesellschaft für Akustik e.V. pp. 1136–1139.

Optimized Driving Functions for Curved Line Source Arrays Using Modeled and Measured Loudspeaker Data

Florian Straube[1], Frank Schultz[2], Michael Makarski[3], Stefan Weinzierl[1]

[1] *Audio Communication Group, TU Berlin, 10587, Berlin, Germany, E-mail: florian.straube@tu-berlin.de*

[2] *Institute of Communications Engineering, University of Rostock, 18119, Rostock, Germany*

[3] *Four Audio GmbH & Co. KG, 52134, Herzogenrath, Germany*

Introduction

Line Source Arrays (LSAs) are used for large-scale sound reinforcement aiming at the synthesis of homogenous wavefronts for the whole audio bandwidth. The deployed loudspeaker cabinets are generally rigged with different tilt angles in order to ensure the coverage of the audience zones and to avoid or reduce undesirable radiation that may be directed at the ceiling, reflective walls or residential areas. By choosing (numerically) optimized driving functions for the individual loudspeakers the homogeneity of the intended wavefront can be further improved [1–7]. This contribution presents an evaluation of driving functions optimized using a goal attainment multiobjective optimization approach as well as a comparison of the synthesized sound fields for modeled and measured loudspeaker data. The complex-directivity point source (CDPS) model-based calculations include far-field radiation patterns of baffled line and circular pistons and the actual loudspeaker data originate from vertical directivity measurements. The analyses are performed for a typical concert venue employing curved LSA setups.

It will be shown with the help of position index plots (PIPs), far-field radiation patterns (FRPs) and driving function index plots (only amplitudes, $\mathrm{DFIP_a}$s) that the model-based multiobjective optimizations provide superior results compared to those obtained via common regularized least-mean-square error optimization approaches. The results are similar for modeled and measured loudspeaker data. In the latter case, however, the quality of the approach critically depends on the spatial resolution of the measured directivity and the correct identification of the spatial aliasing behavior. It is therefore concluded that modeled LSA data are more beneficial than measured directivities for the design and evaluation of appropriate LSA optimization strategies and that this multiobjective optimization approach needs to be extended by additional constraints or the results need to be post-processed for realizable and feasible FIR filters.

LSA setup

A curved LSA setup with a total of $N = 22$ LSA cabinets with $n = 1, 2, ..., N$ is deployed. The front grille's height $\Lambda_{y,\mathrm{LSA}}$ of a single LSA cabinet is set to 0.258 m resulting in an overall LSA length of ca. 5.68 m. γ_n denotes the individual tilt angles and $\mathbf{x_{0,i}}$ denotes the front grille center position of the i-th LSA driver. Detailed information on the geometric configuration can be seen in Fig. 1 and

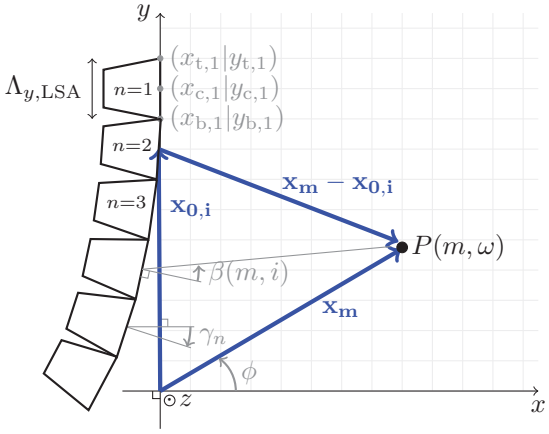

Figure 1: Sketch of the LSA setup under discussion. A total of $N = 22$ LSA cabinets of the height $\Lambda_{y,\mathrm{LSA}} = 0.258\,\mathrm{m}$ is used.

can be found in [8, 9].

Built from two-way cabinets in this paper, the exemplarily chosen LSA consists of $L_{\mathrm{LF}} = 1$ and $L_{\mathrm{HF}} = 1$ vertically stacked, individually controlled drivers per cabinet for the low and the high frequency band (LF, HF). Different loudspeaker sensitivities are assumed in order to obtain realistic sound pressure values, $S_{\mathrm{dB,LF}} = 92$ dB and $S_{\mathrm{dB,HF}} = 112$ dB for vertical radiation in this case. The relation of the pistons' dimensions to the fixed distance between adjacent piston centers which is also known as Active Radiating Factor (ARF) [10, Ch. 3.2], [11] amounts to approximately 0.79. On the one hand, the circular piston model [12, (26.42)] is deployed for LF, the line piston model [12, (26.44)] is deployed for HF and on the other hand measured loudspeaker directivity data are incorporated. For the frequency band crossover, fourth-order Linkwitz-Riley (LR4) filters with a transition frequency $f_{\mathrm{LF,HF}} = 1000$ Hz are used.

Venue Geometry

Following a practical example presented in [5, Sec. 6.1], a multi-stand arena with audience and non-audience sections, i.e. zones to be covered and zones to be avoided, is modeled by a two dimensional slice representation. Only the xy-plane is considered for vertical radiation, cf. Fig. 2. This is a common approach for optimization schemes as the horizontal radiation is assumed to be convenient anyway, cf. [1–7, 13]. $M = 29\,525$ receiver positions with $m = 1, 2, ..., M$ are taken into account. This

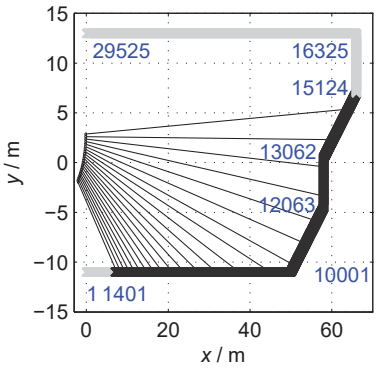

Figure 2: Venue slice within the xy-plane with audience (black) as well as non-audience/avoid (gray) zones and selected index numbers (change of audience/avoid zone and/or polygonal line's segment angle) from M receiver positions.

corresponds to a distance of 0.005 m between the receiver positions ensuring a discretization which approximately equals one fourth of the wavelength at 17.2 kHz.

Calculation Model

Modeling multi-way cabinets the total sound pressure is composed of the sound pressures of the different frequency bands, e.g.

$$P(m,\omega) = P_{\mathrm{LF}}(m,\omega) + P_{\mathrm{HF}}(m,\omega). \tag{1}$$

Since the calculations are performed separately for each frequency band with a subsequent summation, the frequency band indices (LF, HF) are omitted for generalization in the following. The sound field prediction is based on a complex-directivity point source model of baffled piston far-field radiation patterns. Its fundamental equation [14, (11)], [15, Sec. 1.1] reads

$$P(m,\omega) = \sum_{i=1}^{L\,N} G(m,i,\omega)\, D(i,\omega). \tag{2}$$

$P(m,\omega)$ denotes the sound pressure spectrum at the receiver position $\mathbf{x_m}$ with $[P(m,\omega)] = 1\,\mathrm{Pa/Hz}$. $G(m,i,\omega)$ terms the acoustic transfer function (ATF) from the i-th source to the receiver points. The complex driving function spectrum $D(i,\omega)$ with $[D(i,\omega)] = 1\,\mathrm{Pa/Hz}$ of the i-th source is directly proportional to the source's velocity spectrum.

(2) is modified including a loudspeaker sensitivity standardization in order to obtain realistic absolute sound pressure levels (SPLs). Therefore $G(m,i,\omega)$ is considered as a scaled ATF

$$G(m,i,\omega) = H_{\mathrm{post}}(\beta(m,i),\omega)\, \frac{\mathrm{e}^{-\mathrm{j}\,\frac{\omega}{c}\,\|\mathbf{x_m}-\mathbf{x_{0,i}}\|_2}}{\left(\frac{\|\mathbf{x_m}-\mathbf{x_{0,i}}\|_2}{\mathrm{m}}\right)} \times \left(\frac{p_0}{\mathrm{Pa}}\right) 10^{\frac{1}{20}\left(\frac{S_{\mathrm{dB}}(i,\omega)}{\mathrm{dB_{SPL}\,\frac{m}{W}}}\right)} \tag{3}$$

being composed of a specific far-field radiation pattern $H_{\mathrm{post}}(\beta(m,i),\omega)$, the $4\,\pi$-discarded free-field 3D Green's function $\frac{\mathrm{e}^{-\mathrm{j}\,\frac{\omega}{c}\,\|\mathbf{x_m}-\mathbf{x_{0,i}}\|_2}}{\|\mathbf{x_m}-\mathbf{x_{0,i}}\|_2}$ (i.e. the ideal point source), the reference sound pressure p_0 that commonly amounts to $2\times10^{-5}\,\mathrm{Pa}$ in air and the loudspeaker sensitivity $S_{\mathrm{dB}}(i,\omega)$ specifying the SPL in 1 m distance for an electrical input power of 1 W. The sensitivity is assumed to be constant for all drivers and all frequencies per frequency band, i.e. $S_{\mathrm{dB}}(i,\omega) = S_{\mathrm{dB}}$.

Consisting of the signal input spectrum $D_{\mathrm{in}}(i,\omega)$ with $[D_{\mathrm{in}}(i,\omega)] = 1\,\mathrm{Pa/Hz}$, the complex optimized filter $D_{\mathrm{opt}}(i,\omega)$ with $[D_{\mathrm{opt}}(i,\omega)] = 1$ and the complex frequency band crossover as well as high-/lowpass filter $D_{\mathrm{xo}}(\omega)$ with $[D_{\mathrm{xo}}(\omega)] = 1$, thus

$$D(i,\omega) = D_{\mathrm{in}}(i,\omega)\, D_{\mathrm{opt}}(i,\omega)\, D_{\mathrm{xo}}(\omega), \tag{4}$$

an upper limit for the driving function's absolute value can be given as

$$D_{\mathrm{max,dB}}(\omega) \geq \max_i\{D_{\mathrm{in,dB}}(i,\omega)\} + \max_i\{D_{\mathrm{opt,dB}}(i,\omega)\} + D_{\mathrm{xo,dB}}(\omega) \; + D_{\mathrm{hr,dB}}(\omega). \tag{5}$$

This is directly related to the source's maximum electric input power. While the absolute value of the crossover filter usually does not exceed 0 dB, the provided (amplifier) headroom $D_{\mathrm{hr,dB}}(\omega)$ is typically set to e.g. 3 dB.

In line with this modeling, air absorption is neglected, a constant velocity of sound ($c = 343$ m/s) and for the modeled sources infinite, straight baffles and a constant surface velocity are assumed.

Multiobjective Optimization

For the application of optimization algorithms, (2) is rewritten in matrix notation, accounting for all receiver positions M for a single frequency

$$\mathbf{p}(\omega) = \mathbf{G}(\omega)\, \mathbf{d}(\omega) \tag{6}$$

with $\mathbf{p}(\omega)$ denoting the $(M\times1)$ vector of sound pressure spectra at all considered positions $\mathbf{x_m}$, $\mathbf{G}(\omega)$ denoting the $(M\times L\,N)$ (scaled) ATF matrix and $\mathbf{d}(\omega)$ denoting the $(L\,N\times1)$ vector of the complex driving weights at all source positions $\mathbf{x_{0,i}}$ per angular frequency ω. Then, for a desired sound field $\mathbf{p}_{\mathrm{des}}(\omega)$ at the evaluation positions $\mathbf{x_m}$ (6) is solved for the weights $\mathbf{d}(\omega)$. In this case, ca. 3 dB attenuation per distance doubling is requested and a goal attainment multiobjective optimization approach [16] is used. This method is presumably also applied in [5, 6]. Its equation is (cf. [16, (1)] for the general formula)

$$\begin{aligned} &\min_{\zeta,\mathbf{d}(\omega)} \zeta \\ \text{such that:}\quad &\mathbf{F}[\mathbf{d}(\omega)] - \mathbf{w}\,\zeta \leq \mathbf{F}^*[\mathbf{d}(\omega)] \\ \text{subject to:}\quad &|D_{\mathrm{opt}}(i,\omega)| \leq D_{\mathrm{opt,max}}(\omega) \quad \forall i \\ &|D_{\mathrm{opt}}(i,\omega)| \geq D_{\mathrm{opt,min}}(\omega) \quad \forall i \end{aligned} \tag{7}$$

with the vector of objective functions

$$\mathbf{F}[\mathbf{d}(\omega)] = \begin{pmatrix} F_1[\mathbf{d}(\omega)] \\ F_2[\mathbf{d}(\omega)] \end{pmatrix} = \begin{pmatrix} \epsilon_{\mathrm{abs}}(\omega) \\ L_{p,\mathrm{a,na}}(\omega) \end{pmatrix} \tag{8}$$

that shall incorporate the frequency dependent absolute error $\epsilon_{\mathrm{abs}}(\omega)$ (see [9, (16)]) and a frequency dependent measure $L_{p,\mathrm{a,na}}(\omega)$ (see [9, (18)]) that relates

the obtained average levels of the audience zone and the non-audience zone. The latter is established as acoustic contrast in multi-zone sound field synthesis [17, (16)], [18, (2)]. In addition, (7) comprises a set of design goals $\mathbf{F}^*[\mathbf{d}(\omega)]$ for the objective functions and a weighting vector $\mathbf{w}$ with $\mathbf{w} = (w_1, w_2)^{\mathrm{T}}$ to determine a balance between the different objectives. Note that $\max_{\omega}\{|D_{\mathrm{opt}}(i,\omega)|\}$ provides quantitative information on the common trade-off between the increase of the sound field's homogeneity and the decrease of the maximum SPL output.

Discussion

In Fig. 3 the PIPs, i.e. the SPL spectra at all control positions $\mathbf{x_m}$, the FRPs, i.e. the polar patterns for radiating angles $|\phi| \leq 90°$ as an isobar plot over all evaluated frequencies, and the $\mathrm{DFIP_a}$s, i.e. the magnitudes over frequency that have to be applied to the individual sources, can be seen. For the chosen LSA setup with modeled as well as measured loudspeaker data, the optimizations are performed separately for each frequency of a logarithmically spaced frequency vector with $f_{\mathrm{start}} = 200$ Hz, $f_{\mathrm{stop}} = 20$ kHz and 1/36th octave resolution. The aliasing frequency f_{alias} referring to the spatial sampling condition $\Delta y \leq \frac{c}{2f}$ for straight arrays is ca. 664.73 Hz.

The PIPs show that the desired sound field is quite sufficiently obtained for LF and for some extent also for HF. Due to the single LF piston (vertically) per cabinet and the large waveguide, (complex) optimized filters are not very meaningful to be applied for high frequencies for this LSA design. For frequencies below roughly 2 kHz mostly the non-audience positions are just scarcely fed and a homogenous audience coverage is provided. Above this frequency the sound field is severely corrupted by spatial aliasing and the sound is also radiated into the regions that are to be avoided. In the FRPs, this is also visible on the basis of the grating lobes for the high frequencies. Mainly the sources in the middle of the LSAs are loaded for frequencies larger than f_{alias}, whereas the drivers' loads are quite balanced below this value, cf. Fig. 3e, Fig. 3f. Note that the DFIP phases as group delays are not depicted here.

Conclusion

The model-based multiobjective optimizations provide superior results compared to those obtained via common regularized least-mean-square error optimization approaches (cf. [9]) as the distinct drivers' loads can be controlled individually. Using the CDPS model for both modeled and measured loudspeaker data, the results are very similar for the LF as well as the HF range, remarkable differences can be observed only for HF. These mainly involve the correct identification of the spatial aliasing behavior since the spatial resolution of the measured loudspeaker directivity may not be sufficient and because of the specific waveguide characteristics. For the design and evaluation of appropriate LSA optimization strategies it may be therefore favorable to focus on modeled loudspeaker data, whereas the measured loudspeaker data do not necessarily have to be utilized before the drive computation of practical LSA setups. It is also recommendable to limit the bandwidth of numerical optimizations, depending on the array length and the spatial aliasing frequency. The calculated driving functions could be further improved by frequency smoothing in order to allow only small changes between nearby frequencies. A technically or psychoacoustically-motivated constraint for the DFIP phases as group delays (e.g. linear phases) should be added for realizable and feasible FIR filters. An alternative approach may be using an amplitude shading, bearing on the LSA and receiver geometry and being numerically refined.

References

[1] van Beuningen, G.W.J.; Start, E.W. (2000): "Optimizing directivity properties of DSP controlled loudspeaker arrays." In: *Proc. of the Inst. of Acoustics: Reproduced Sound*, **22**(6):17–37.

[2] Thompson, A. (2008): "Real world line array optimisation." In: *Proc. of the Institute of Acoustics*, **30**(6).

[3] Thompson, A. (2009): "Improved methods for controlling touring loudspeaker arrays." In: *Proc. of the 127th Audio Eng. Soc. Conv., New York*, #7828.

[4] Terrell, M.; Sandler, M. (2010): "Optimising the controls of a homogenous loudspeaker array." In: *Proc. of the 129th Audio Eng. Soc. Conv., San Francisco*, #8159.

[5] Thompson, A.; Baird, J.; Webb, B. (2011): "Numerically optimised touring loudspeaker arrays - Practical applications." In: *Proc. of the 131st Audio Eng. Soc. Conv., New York*, #8511.

[6] Feistel, S.; Sempf, M.; Köhler, K.; Schmalle, H. (2013): "Adapting loudspeaker array radiation to the venue using numerical optimization of FIR filters." In: *Proc. of the 135th Audio Eng. Soc. Conv., New York*, #8937.

[7] Thompson, A.; Luzarraga, J. (2013): "Drive granularity for straight and curved loudspeaker arrays." In: *Proc. of the Inst. of Acoustics*, **35**(2):210–218.

[8] Straube, F.; Schultz, F.; Weinzierl, S. (2015): "On the effect of spatial discretization of curved Line Source Arrays." In: *Fortschritte der Akustik: Tagungsband d. 41. DAGA, Nuremberg*, 459–462.

[9] Straube, F.; Schultz, F.; Makarski, M.; Spors, S.; Weinzierl, S. (2015): "Evaluation strategies for the optimization of Line Source Arrays." In: *Proc. of the 59th Audio Eng. Soc. Int. Conf. on Sound Reinforcement, Montreal.*

[10] Urban, M.; Heil, C.; Bauman, P. (2003): "Wavefront Sculpture Technology." In: *J. Audio Eng. Soc.*, **51**(10):912–932.

[11] Schultz, F.; Straube, F.; Spors, S. (2015): "Discussion of the Wavefront Sculpture Technology criteria for straight line arrays." In: *Proc. of the 138th Audio Eng. Soc. Conv., Warsaw*, #9323.

[12] Skudrzyk, E. (1971): *The Foundations of Acoustics.* New York: Springer.

[13] Thompson, A. (2006): "Line array splay angle optimisation." In: *Proc. of the Inst. of Acoustics*, **28**(8):135–148.

[14] Feistel, S.; Thompson, A.; Ahnert, W. (2009): "Methods and limitations of line source simulation." In: *J. Audio Eng. Soc.*, **57**(6):379–402.

[15] Meyer, P.; Schwenke, R. (2003): "Comparison of the directional point source model and BEM model for arrayed loudspeakers." In: *Proc. of the Institute of Acoustics*, **25**(4).

[16] Gembicki, F.W.; Haimes, Y.Y. (1975): "Approach to performance and sensitivity multiobjective optimization: The goal attainment method." In: *IEEE Trans. on Automatic Control*, **20**(6):769–771.

[17] Choi, J.W.; Kim, Y.H. (2002): "Generation of an acoustically bright zone with an illuminated region using multiple sources." In: *J. Acoust. Soc. Am.*, **111**(4):1695–1700.

[18] Coleman, P.; Jackson, P.J.B.; Olik, M.; Møller, M.; Olsen, M.; Pedersen, J.A. (2014): "Acoustic contrast, planarity and robustness of sound zone methods using a circular loudspeaker array." In: *J. Acoust. Soc. Am.*, **135**(4):1929–1940.

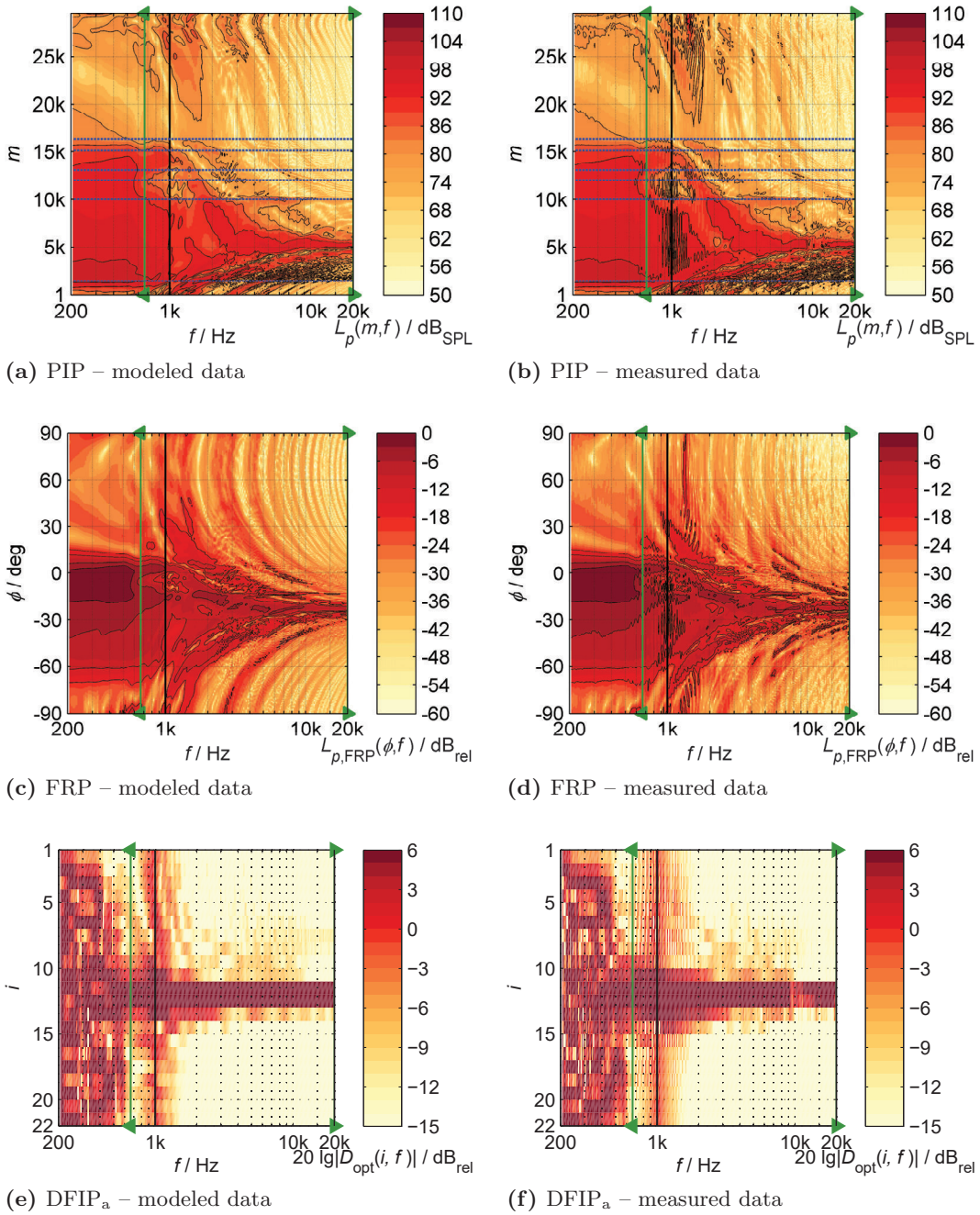

(a) PIP – modeled data

(b) PIP – measured data

(c) FRP – modeled data

(d) FRP – measured data

(e) DFIP$_a$ – modeled data

(f) DFIP$_a$ – measured data

Figure 3: Position index plots (PIPs, first row), far-field radiation patterns (FRPs, second row) and driving function index plots (DFIP$_a$s, only amplitudes) for an optimized drive of the exemplarily chosen LSA design. The optimizations with $\mathbf{F}^*[\mathbf{d}(\omega)] = (10^{-6}\,\mathrm{Pa}^2, 15\,\mathrm{dB_{rel}})^\mathrm{T}$, $\mathbf{w} = (1, -1/0.3)^\mathrm{T}$ and $D_{\mathrm{opt,max,dB}}(\omega) = 6\,\mathrm{dB_{rel}}$, $D_{\mathrm{opt,min,dB}}(\omega) = -15\,\mathrm{dB_{rel}}$ for all drivers are based on modeled (left) and measured loudspeaker directivity data (right). Isobars are included for the PIPs from 80 dB$_{SPL}$ to 110 dB$_{SPL}$ in 6 dB steps and for the FRPs for -3 dB$_{rel}$, -6 dB$_{rel}$, -12 dB$_{rel}$ and -18 dB$_{rel}$. The crossover frequency $f_{LF,HF}$ (black, vertical) and the spatial aliasing frequency f_{alias} of an equivalent straight array (green with arrows) are charted for orientation.